ELSEVIER

Medical Engineering & Physics 23 (2001) 329–346

Medical Engineering & Physics

www.elsevier.com/locate/medengphy

The electrochemical oxide growth behaviour on titanium in acid and alkaline electrolytes

Young-Taeg Sul [a,*], Carina B. Johansson [a], Yongsoo Jeong [b], Tomas Albrektsson [a]

[a] *Department of Biomaterials/Handicap Research, Institute for Surgical Science, University of Göteborg, Göteborg, Sweden*
[b] *Surface Engineering Department, Korea Institute of Machinery and Materials, 66 Sangnam-dong, Changwon, Kyungnam, South Korea 641 010*

Received 19 October 2000; received in revised form 21 March 2001; accepted 26 April 2001

Abstract

Titanium implants have a thin oxide surface layer. The properties of this oxide layer may explain the good biocompatibility of titanium implants. Anodic oxidation results in a thickening of the oxide film, with possible improved biocompatability of anodized implants. The aim of the present study was twofold: (1) firstly, to characterize the growth behaviour of galvanostatically prepared anodic oxide films on commercially pure (c.p.) titanium and (2) secondly, to establish a better understanding of the electroche0mical growth behaviour of anodic oxide on commercially pure titanium (ASTM grade 1) after changes of the electrochemical parameters in acetic acid, phosphoric acid, calcium hydroxide, and sodium hydroxide under galvanostatic anodizing mode. The oxide thickness was measured by Ar sputter etching in Auger Electron spectroscopy (AES) and the colours were estimated by an L*a*b* system (lightness, hue and saturation) using a spectrophotometer. In the first part of our study, it was demonstrated that the interference colours were useful to identify the thickness of titanium oxide. It was also found that the anodic forming voltages with slope (dV/dt) in acid electrolytes were higher than in alkaline electrolytes. Each of the used electrolytes demonstrates an intrinsically specific growth constant (nm/V) in the range of 1.4–2.78 nm/V. In the second part of our study we found, as a general trend, that an increase of electrolyte concentration and electrolyte temperature respectively decreases the anodic forming voltage, the anodic forming rate (nm/s) and the current efficiency ($nm.cm^2/C$), while an increase of the current density and the surface area ratio of the anode to cathode increase the anodic forming voltage, the anodic forming rate and the current efficiency. The effects of electrolyte concentration, electrolyte temperature, and agitation speed were explained on the basis of the model of the electrical double layer.

Keywords: Titanium implants; Anodic oxidation; Oxide growth behaviours; Electrochemical parameters

1. Introduction

The concept of osseointegration was originally introduced by Brånemark et al. in 1977 [1] and the importance of the implant surface properties for a successful osseointegration was first pointed out by Albrektsson and co-workers in 1981 [2].

In general, it is known that titanium metal is spontaneously covered by a surface oxide of 1.5–10 nm thickness, if in air at room temperature [3]. The outer covering oxide of a turned titanium implant consists mainly of TiO_2 [4,5], and is basically amorphous in crystal structure and morphologically homogeneous [6]. Moreover, this thin oxide surface layer results in an excellent resistance to corrosion indicated by: electrochemically a low level of electronic conductivity [7], thermodynamically great stability [8,9] and low ion-formation tendency in aqueous environments [10]. These properties of the natural oxide layer may be the reasons for the excellent biocompatibility leading to favourable tissue responses to titanium implants in comparison to many other metal implants [11], since primary interaction between implant and biological environment at the implant–tissue interface is dependent on the surface properties of the titanium oxide layer and not on the bulk titanium itself.

To improve the bone tissue response to titanium

* Corresponding author. Tel.: +46-31-773-2950 fax: +46-31-773-2941.
E-mail address: young-taeg.sul@hkf.gu.se (Y.-T. Sul).

1350-4533/01/$20.00
PII: S1350-4533(01)00050-9

implants, some topographical surface modifications have been demonstrated as quite effective, at least in animal models [12–15]. Thus, blasted surfaces of an average roughness (Sa) of 1.5 μm have resulted in significantly stronger bone responses than have smoother and rougher surfaces [16]. However, surface roughness changes at the nanometer level of resolution, generally seen with oxidized implants compared to controls, have not been verified to influence the bone response, to the level of our current knowledge.

Electrochemical parameters critically influence on the oxide properties/growth behaviours of the titanium metal. Growth of the oxide thickness results in systemic changes of the surface topography, particularly in the surface pore configuration [17], whereas an anionic incorporation into oxide films will alter the chemical compositon [18] as well as the crystal structures of the titanium oxide, the latter examplified by anatase, rutile, and even the rare brukite type [19–22]. However, results reported in the literature give a rather complex and somewhat contradictory picture on the solid state properties and the electrochemical growth behaviour of anodic oxide films [23–48]. It is generally known that titanium behaves as a typical valve metal for which oxide growth involves field-assisted migration of ions through the oxide films and for the thickness of the anodic oxide to follow Faraday's law [23–27]. Moreover, the growth constant values of anodic film are variable according to many reports [38–41]. Growth constant considerably influences the surface properties of anodic oxide films such as defect concentration profile [42] as well as the formation of an intermediate suboxide TiO_{2-x} layer between the deep TiO layer of the titanium substrate and the more superficial TiO_2 layer of the titanium oxide [43]. During anodic oxidation of titanium metal, gas evolution (O_2 and H_2) is usually observed, which contributes to reduce the current efficiency to anodic oxide growth [18–32]. Furthermore, the structure of anodic film is changed from amorphous to crystalline phase, e.g. anatase, brukite, and rutile, which occurs above 'a critical' oxide thickness [33,34]. This crystallographic transformation is closely related to the breakdown, which is dependent on the electrochemical parameters such as the electrolyte concentration (or activity) [34,35] and the current density [36,37]. Disagreements between various studies may arise from varying surface preparations and growth conditions examplified by the current density, the chemical composition (concentration), and the electrolyte temperature.

The present study is one of several investigations. In the first part of this in vitro study our aim is to investigate the characteristic behaviour of the galvanostatic anodic oxide growth prepared in several electrolytes on commercially pure (c.p.) titanium (ASTM grade 1) and to analyse the colours of the resultant titanium oxide films. In the second part, the present study aims to present a better understanding of the electrochemical growth behaviour of the galvanostatic anodic oxide on commercially pure (ASTM grade 1) accompanied by changing the electrochemical parameters such as the electrolyte concentration, the applied current density, the electrolyte temperature, the agitation speed, and the surface area ratios of cathode to anode.

2. Materials and methods

2.1. Preparation of the samples

Commercially pure (c.p.) titanium (99.6 at %, ASTM grade 1) was used for preparing the samples as plates and screw type anodes. The plate type was 30×10×1.0 mm with a small handle of 30×2.5×1.0 mm which during anodizing was masked with teflon tape. The screw type was a clinical oral implant that had a length of 18 mm and a diameter of 3.75 mm. The screw type anode was held by a teflon-encased screw holder. The electrolytic cell consisted of double Pyrex glasses with a cooling jacket. The titanium anode was suspended in the centre of the cell by use of a sample holder. In the second part of the study, commercially pure (c.p) titanium (ASTM grade 1 and grade 2) was prepared for disc type anodes that consisted of four titanium rods attached by screwing into prepared holes of a titanium disc that was subsequently embedded in resin. Before resin embedding, each titanium rod was masked with teflon tape. This double sealing aims to prevent the leakage of electrolyte into the titanium anode and to make it possible to accurately calculate the surface area of the titanium anode, eventually to make sure of the applied current density. Each titanium rod had a cross-sectional area of 0.125 cm^2. During anodizing this multi-anode was held by a sample holder encased with teflon. The titanium multi-anode is schematically illustrated with the anodizing apparatus in Fig. 1. All specimens were abraded by SiC paper in successive grades from 300 to 800 grit (Struers, Denmark), and then ultrasonically cleaned in detergent solutions and dried in an oven at 50°C for 24 h. Two platinum plates having the surface area of 80 cm^2 were used as counter electrodes at both sides of the titanium anode. In the first part the surface area ratios of the titanium anode versus the counter electrodes were 3.5% for the screw type and 8.5% for the plate type of anode. In the second part the surface area ratio of the titanium anode versus the counter electrode was less than 0.625%. A dc power supply interfaced with an IBM computer (Hobang Electronics, Korea) was used (Fig. 1). Currents and voltages were continuously recorded at intervals of 0.5 s by an IBM computer interfaced with the power supply. The content of ripple was controlled to less than 0.1%. Five different electrolytes were used: sulphuric acid, acetic acid, phosphoric acid, calcium hydroxide, and sodium

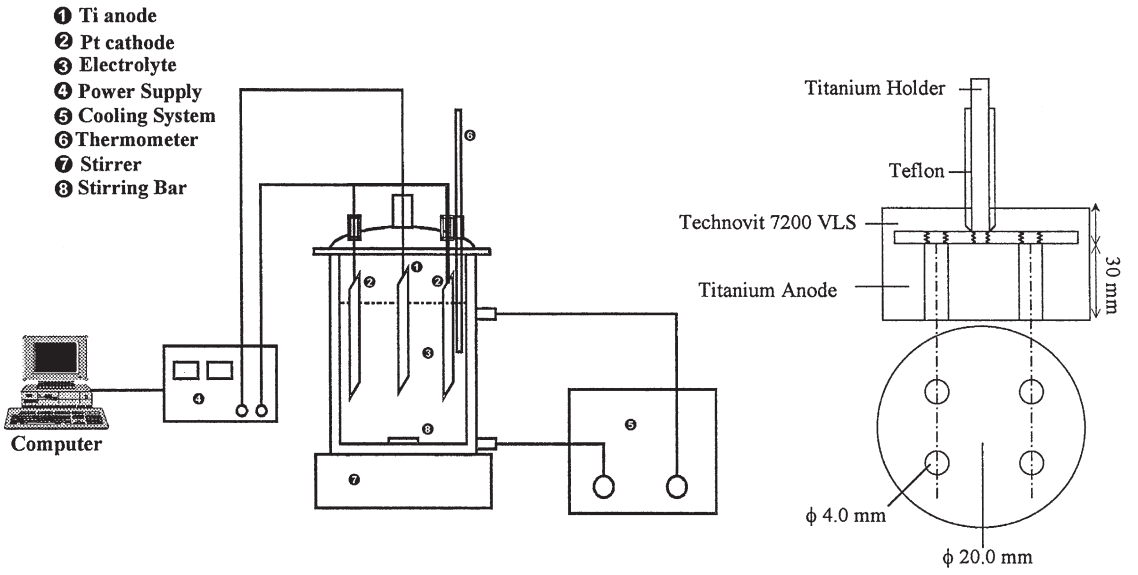

Fig. 1. Schematic diagram of the anodizing apparatus, electrolytic cell and multi-titanium electrode.

hydroxide. The applied voltages were given at the range of 20–130 V and the current density at 5–40 mA/cm^2. The agitation speed was in the range of 250–800 rpm. The temperature was controlled in the range of 14–42°C. The temperature rise due to the exothermic anodic reaction was controlled to less than 2°C. The anodic oxidation was performed in a galvanostatic mode.

2.2. Analysis

Altogether 59 samples were measured with Auger Electron Microscopy (AES, Physical Electronics, model PHI 650). The growth behaviour of galvanostatic anodic oxide film was analysed in terms of the anodic oxide thickness, the oxide growth constant (nm/V), the current efficiency (nm.cm^2/C), and the anodic forming rate (nm/s). The reproducibility of the electrochemical behaviour of the electrolytes employed in this study was very stable as approximately 98% of anodic forming voltage at 100 V in acid electrolytes and at 60 V in alkaline electrolytes. The colours of the anodized titanium oxide film were estimated by an L*a*b* system (the lightness, the hue, the saturation) using a spectrophotometer CM-3500d (Minolta, Japan) with a light source of D 65. Illumination angle was 45° and view angle was 0°. The colours of titanium oxide were analysed in terms of the used electrochemical parameters and a corresponding oxide thickness. Depth profile of the anodic oxide thickness were performed by continuous sputter etching with 4 keV Ar ion in AES. Measuring area was at a diameter of 2.5×4.0 μm. For the determination of the oxide thickness, the relation $d=v_0t_d$, where d is the film thickness, v_0 is the sputter rate, and t_d, is the sputtering time when the oxygen peak amplitude at the metal–oxide interface has decreased to 50% of its steady state values in the oxide [49]. To be precise, calibration of the sputtering rate was double-checked by two reference materials of 100 nm of SiO_2 and 91.8 nm of TiO_2. The reference TiO_2 film was deposited on (100) Si by MOCVD (Metal Organic Chemical Vapor Deposition). By using Ellipsometry, this reference TiO_2 film was characterized as 91.8 nm in the oxide thickness and 2.199 in the refractive index with values between 2.0 for amorphous type and 2.5 for anatase type of TiO_2 crystal structure. With the quoted two reference materials, the sputtering rate is induced at about 7.1 nm/min. To assess the experimental standard deviation of the oxide thickness measured in the present study, the depth profile was performed on the randomly selected three specimens before and after anodic oxidation. The experimental standard deviation in the oxide thickness was 0.042 for 9.83 nm of the native oxide thickness and 4.0 for 109.1 nm of the anodic oxide thickness (Fig. 2). Hereby, a possible maximum inaccurracy in the present study in calculation of the galvanostatic anodic oxide thickness measured by AES can be assessed at about 3.7% and in the stability of voltage and current due to systemic error at 0.1%.

3. Results

3.1. The colours of the galvanostatic anodic oxide films

Colouring of the resultant titanium anodic oxide films was the most prominent optical change during galvanostatic anodizing. All the results are summarized in Table 1. Fig. 3 shows various colours of the anodic oxide film prepared on the clinical implant specimens. Fig. 4 shows

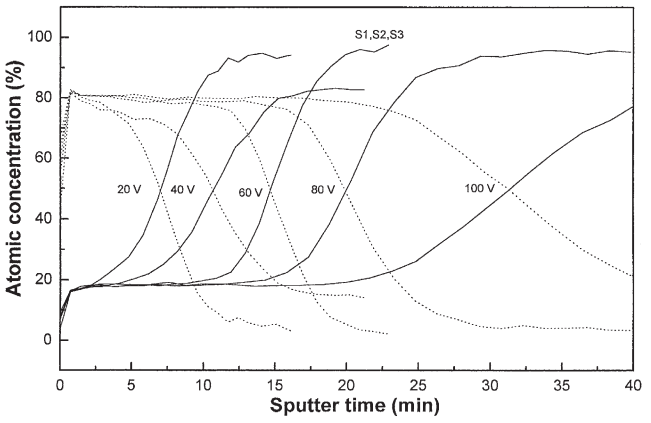

Fig. 2. AES depth profiling of the anodic oxide films grown in 0.1 M sulphuric acid at 20, 40, 60, 80 and 100 V. Measurements on three randomly selected areas (S1, S2 and S3) of the anodic film formed at 60 V, showed uniformity of oxide thickness (109±4 nm). The relative atomic concentration (%) in Ti and O elements is plotted.

that the colouring of the titanium oxide films is expressed in relation to the anodic forming voltage and the galvanostatic anodic oxide thickness. From all the detailed figures in Table 1, it was found that the colours of the anodic titanium oxide expressed by the hue (a* value), in principle, was dominated by the anodic oxide thickness within the range of which the anodic forming voltage increased almost linearly with the anodizing time. However, not only the value of a* but also the L and b* showed considerable differences according to the electrolytes employed even though the anodic oxide thickness as well as the forming voltage was the same. It was also found that even though the anodic oxide films are prepared at the same forming voltage and the same electrolyte as investigated in acetic acid (A1, A2 and A3 in Table 1), the corresponding colours of the titanium oxide vary by changing the current density and the electrolyte concentration.

3.2. The nature of the electrolytes and the characteristics of the galvanostatic oxide film growth

Fig. 5 shows typical voltage-to-time transients (d*V*/d*t*) during growth of the galvanostatic anodic oxide film on the plate type titanium. At the beginning of anodizing, the anodic forming voltage goes up linearly with time up to a certain point of time in the range of approximately 10–20 s, whereafter anodic forming voltage transient with slope (d*V*/d*t*) decreases gradually with anodizing time in all the used electrolytes. Depending on the used electrolytes, however, the growth behaviour of galvanostatic anodic oxide is very complicated and appeared quantitatively differently at various stepwise potential increase from 20 to 100 V. The electrochemical parameters and the detailed results used in the first part of the present study are summarized in Table 1.

3.2.1. Sulphuric acid

The electrochemical behaviour and galvanostatic anodic oxide growth rate was estimated in 1.0 M sulphuric acid (pH 0.99, conductivity 10.39 μs/cm) at a stepwise potential increase of 10 up to 130 V on the plate type of titanium anode. As seen in Fig. 5 (S curve), the voltage to time curve presented three different phases of the anodic forming voltage transient with slope (d*V*/d*t*). Anodic forming voltage increased straight up to about 40 V in the first stage, thereafter slightly decreased up to about 70 V in the second stage, and finally it moved with the lowest voltage to time gradient. Accordingly, as shown in Fig. 6, the anodic oxide thickness increased linearly with increase of applied voltage up to 70 V of forming voltage. After 70 V of forming voltage, anodic oxide thickness increased nearly exponentially with an increase of the applied voltage. In addition, it is clearly found that the anodic oxide thickness in sulphuric acid was the thickest among all the used electrolytes in any given anodic forming voltage up to 100 V, except for the situation of the calcium hydroxide at 60 V which was already at steady state of the anodic forming voltage. Fig. 7 shows the relationship between the growth constant (α, nm/V) of anodic oxide film and forming voltage. Overall, the growth constant values (nm/V) demonstrated two qualitatively different behaviours before and after a critical voltage point/range, namely a descending stage with the mean value of 1.97 nm/V (±0.26) up to 70 V and an ascending stage with the mean value of 2.14 nm/V (±0.43) up to 130 V. The current efficiency (nm.cm^2/C) demonstrated three divisions of different transient values with a mean value of 1124 nm.cm^2/C (±194) up to 40 V, 874 nm.cm^2/C (±196) up to 60 V, and 531 nm.cm^2/C (±138) up to 100 V (S in Fig. 8). Furthermore, as shown in Fig. 8, it is also clearly detected that in contrast to the behaviours of the oxide thickness and the oxide growth constant, the current efficiency (nm.cm^2/C) in sulphuric acid was the lowest among all the used acid electrolytes at any given voltage up to 100 V. Fig. 9 shows that the oxide forming rate decreases exponentially with the anodizing time.

3.2.2. Acetic acid

Fig. 5 (A1 curve) shows the voltage-to-time transients (d*V*/d*t*) in 0.1 M acetic acid at 5 mA/cm^2. In contrast to 1.0 M sulphuric acid, however, the anodic oxide thickness linearly increased with an increase of anodic forming voltage up to 100 V (A1 in Fig. 6). The growth constant of anodic oxide films linearly decreased with increases of the anodic forming voltage (A1 in Fig. 7). The current efficiency (nm.cm^2/C) most rapidly decreased with increases of anodic forming voltage between all electrolytes (A1 in Fig. 8). As shown in Fig. 9, the anodic oxide forming rate decreased exponentially with the anodizing time examplified sulphuric acid.

Table 1
Summary of the electrochemical parameters and the corresponding interference colours[a]

Volt. (V)	Time (s)	Charge ($C/cm^2/C$)	Current efficiency ($nm.cm^2/C$)	Oxide thickness (nm)	Growth constant (nm/V)	Anodic oxide forming rate (nm/s)	L	a*	b*	Interference colour
Sulphuric acid (S), 1.0 M, 15 mA/cm²										
22	2.5	0.0375	1448	54.3	2.47	21.7	41.1717	9.6489	−18.246	Dark purple
36	4	0.06	1133	68	1.89	17	56.9717	−5.891	−19.1665	Bluish purple
40	5	0.075	1092	81.9	2.04	16.4	59.3126	−7.6167	−16.1787	Blue
50	7.5	0.1125	820	93	1.86	12.4	73.8705	−7.8617	−2.87	Bright blue
60	10	0.15	711	109.1	1.82	10.9	76.4356	−6.2837	26.077	Bluish yellow
70	13.5	0.202	615	124.3	1.75	9.2	70.7001	4.9994	46.7447	Yellow
80	18.5	0.2775	532	147.7	1.85	8	60.8176	22.3475	22.0385	Bright orange
90	26.5	0.3975	438	174	1.93	6.6	50.5267	23.736	−13.3727	Scarlet
100	44.5	0.6675	363	242.4	2.42	5.4	52.4587	−0.1428	−8.731	Green
130	156	2.34	154	361.5	2.78	2.3	50.8179	0.4009	0.3345	Gray
Acetic acid (A1), 0.1 M, 5 mA/cm²										
22	2	0.01	5180	51.8	2.35	25.9	36.447	18.4299	−10.7031	Dark orange
40	7	0.035	2291	80.2	2	11.5	68.1599	−9.3634	−9.0814	Yellowish blue
60	16	0.08	1275	102	1.7	6.4	74.4682	0.7943	7.8532	–
80	28	0.14	839	117.5	1.47	4.2	79.9248	−6.4493	15.433	Bright yellow
100	52	0.26	540	140.4	1.4	2.7	67.6114	23.105	18.8424	Yellow+red
Acetic acid (A2), 1.0 M, 5 mA/cm²										
40	11.5	0.058	1224	71	1.78	6.2	51.9702	−3.6051	−24.3608	Blue
60	27	0.135	834	112.6	1.87	4.2	79.8537	−6.9609	3.6863	Bright green
80	47	0.235	631	148.4	1.85	3.2	73.6822	3.0404	38.2472	Yellow
100	97	0.485	484	234.5	2.34	2.4	57.2785	8.1966	−15.7501	Purple
Acetic acid (A3), 1.0 M, 10 mA/cm²										
60	9	0.09	962	86.6	1.44	9.6	74.3474	−8.745	−5.7132	Bright blue
80	17.5	0.175	771	134.9	1.68	7.7	78.2366	−3.3224	29.3426	Bright yellow
100	31.5	0.315	606	191	1.91	6.1	60.904	23.7515	−1.5605	Bright scarlet

(continued on next page)

Table 1 (*continued*)

Volt. (V)	Time (s)	Charge ($C/cm^2/C$)	Current efficiency ($nm.cm^2/C$)	Oxide thickness (nm)	Growth constant (nm/V)	Anodic oxide forming rate (nm/s)	L	a*	b*	Interference colour
Phosphoric acid (P), 1.0 M, 5 mA/cm²										
20	6.5	0.0325	1406	45.7	2.29	7	43.6603	15.1477	21.2193	Orange
40	9.5	0.0475	1416	67.3	1.68	7	59.5105	−5.8653	−11.9458	Dark blue (greenish)
60	12.5	0.0625	1547	96.7	1.61	7.6	69.7461	−5.5813	−1.9076	Blue+gray
80	17	0.085	1412	120	1.5	7	79.4502	−3.9878	17.7626	Bright yellow green
100	23	0.115	1339	154	1.54	6.7	70.3265	11.233	25.2445	Reddish yellow
Calcium hydroxide (Ca), 1.0 M, 5 m/cm²										
20	7	0.035	1254	43.9	2.19	6.3	44.8987	14.6415	14.5794	Dark orange
40	28	0.14	556	77.9	1.94	2.8	62.6144	−8.1538	−20.0518	Dark blue
60	101	0.505	199	100.4	1.67	1	80.1022	−5.2394	10.4543	Blueish green
Sodium hydroxide (Na), 0.1 M, 5 mA/cm²										
20	8	0.04	1065	42.6	2.13	5.3	41.3038	16.6682	1.8185	Dark yellowish red
40	28	0.14	483	67.6	1.69	2.4	66.0577	−9.446	−17.2758	Bright blue
60	236	1.18	119	140.6	2.34	0.6	75.6012	−3.0708	18.6543	Light yellow

[a] L represented the lightness of the reflected light from the specimen, a* the hue and b * the saturation.

Fig. 3. Colouring of the clinical titanium implants prepared by galvanostatic oxidation; the native oxide film (reference colour) of a clinical screw implant to the left, the interference colours consecutively anodized at 20, 40, 80, 100, 180 and 200 V to the right, in 0.5 M tartaric acid.

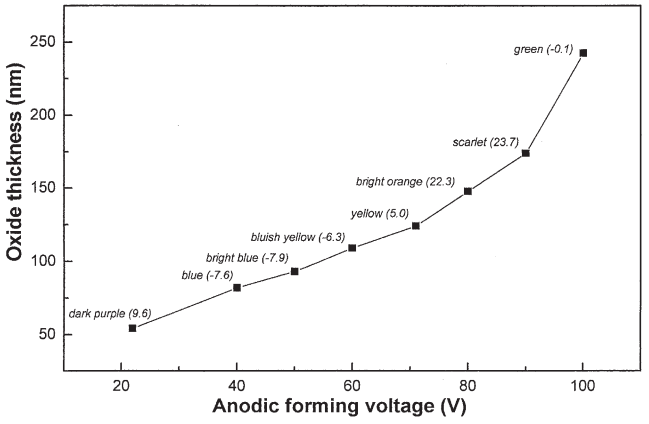

Fig. 4. The interference colours formed on on the plate type of titanium anode in 1.0 M sulphuric acid (pH 0.99, conductivity 10.39 μs/cm) are presented with relation to the galvanostatic anodic oxide thickness and the anodic forming voltage from 20 to 130 V. Numbers in parentheses referred to a* value of L a* b* colour measuring system.

3.2.3. Phosphoric acid

The voltage-to-time transient curve of phosphoric acid in Fig. 5 (P curve) demonstrates the highest value of anodic forming voltage in phosphoric acid and nearly a constant slope (dV/dt). The anodic oxide thicknesses linearly increased with an increase of the forming voltage up to 100 V (P in Fig. 6). However, the growth constant (nm/V) decreased from 2.29 nm/V at 20 V to 1.54 nm/V at 100 V (P in Fig. 7). As shown in Fig. 8, the current efficiency (nm.cm^2/C) in phosphoric acid was nearly constant at any given voltage from 20 to 100 V, whereas the current efficiency in all other electrolytes decreased. This behaviour is correspondent to behaviour of the voltage to time characteristic curve as shown in Fig. 5. The mean value of the current efficiency is 1424 nm.cm^2/C (±75). As a consequence, as shown in Fig. 9, the anodic oxide forming rate in phosphoric acid presents a specific behaviour: as for all the electrolytes

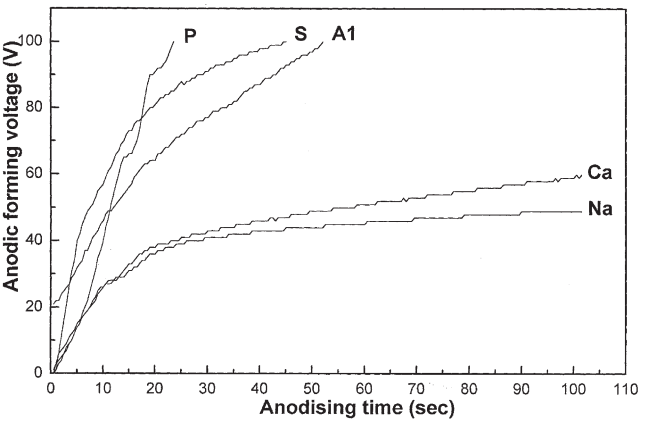

Fig. 5. Typical voltage to time characterics on a titanium electrode. The anodic forming voltage (V) is plotted as a function of time during galvanostatic anodizing in five electrolytes: P=1.0 M phosphoric acid at 5 mA/cm^2; S=1.0 M sulphuric acid at 15 mA/cm^2; Al=0.1 M acetic acid at 5 mA/cm^2; Ca=0.1 M calcium hydroxide at 5 mA/cm^2; Na=0.1 M sodium hydroxide at 5 mA/cm^2.

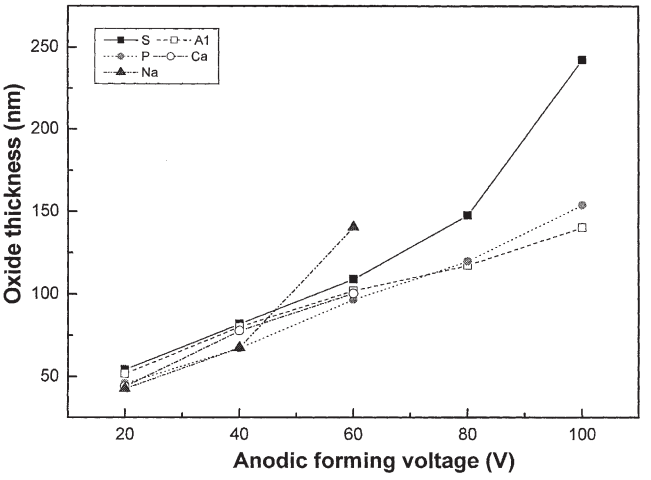

Fig. 6. Relationship between the oxide thickness and the anodic forming voltage up to 100 V: P=1.0 M phosphoric acid at 5 mA/cm^2; S=1.0 M sulphuric acid at 15 mA/cm^2; Al=0.1 M acetic acid at 5 mA/cm^2; Ca=0.1 M calcium hydroxide at 5 mA/cm^2; Na=0.1 M sodium hydroxide at 5 mA/cm^2.

used in the present study, the oxide forming rate decreased with the anodizing time, whereas the anodic forming rate in phosphoric acid was nearly constant with a mean value of 7.0 nm/s (±0.32) for any given anodizing time.

3.2.4. Calcium hydroxide

The anodic forming voltage in alkaline electrolytes yields much lower in comparison to acid electrolytes (Ca and Na in Fig. 5). The anodic forming voltage transient with slope (dV/dt) in 0.1 M calcium hydroxide decreases prominently after about 40 V, subsequently it almost reaches a steady-state (Ca in Fig. 5). As shown in Fig. 6, however, anodic oxide thickness linearly increases

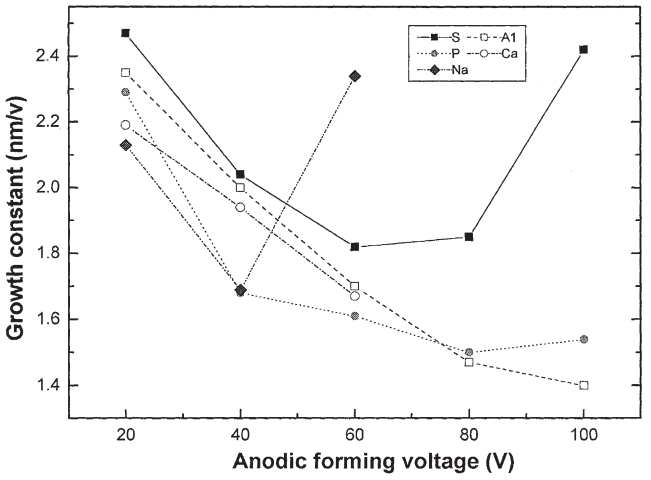

Fig. 7. Dependence of the growth constant on the nature of the used electrolytes and the anodic forming voltage. The growth constant clearly demonstrates two different characteristics: descending stage and ascending stage relevant to the anodic forming voltage. The abbreviations were presented by the used electrochemical parameters as before.

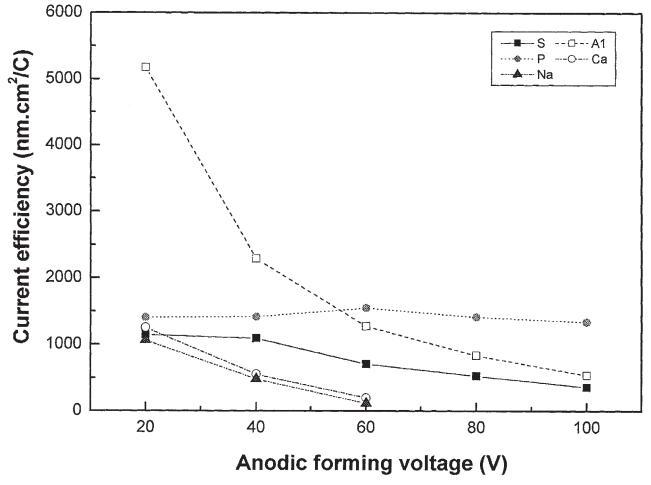

Fig. 8. The current efficiency is presented as a function of the anodic forming voltage. The abbreviations were presented by the used electrochemical parameters as before.

with an increase of the forming voltage up to 60 V. The growth constant (nm/V) decreased with increase of forming voltage up to 60 V (Ca in Fig. 7). The current efficiency (nm.cm^2/C) was much lower in comparison to acid electrolytes (Fig. 8). Anodic oxide forming rate (nm/s) was also lower in comparison to acid electrolytes and decreased with the anodizing time (Fig. 9).

3.2.5. Sodium hydroxide

Fig. 5 (Na curve) shows that the anodic forming voltage of 0.1 M sodium hydroxide is the lowest in all electrolytes. There was big difference in anodizing time (101 vs 236 s) up to 60 V between calcium hydroxide and sodium hydroxide. However, the anodic oxide thickness

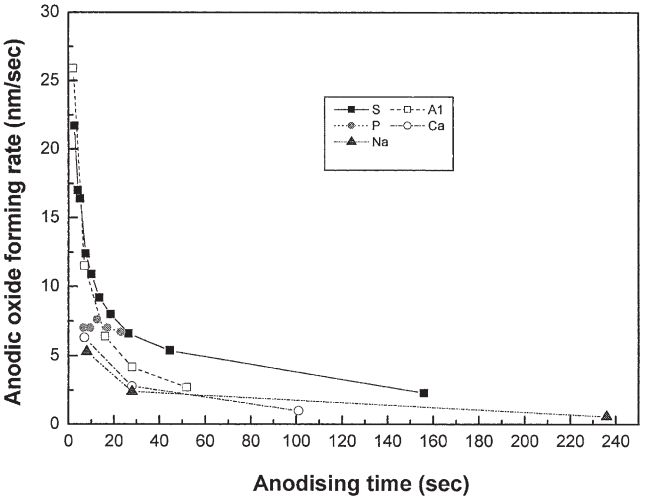

Fig. 9. The anodic oxide forming rate is presented as a function of anodizing time. The abbreviations were presented by the used electrochemical parameters as before.

linearly increases with an increase of anodic forming voltage up to 60 V (Na in Fig. 6). The growth constant (nm/V) linearly decreased (Na in Fig. 7). The current efficiency and anodic oxide forming rate behave quite similarly as compared to calcium hydroxide (Figs. 8 and 9). It is clearly found in the present study that the alkaline electrolytes yield very low anodic forming voltage, oxide growth constant (nm/V), current efficiency (nm.cm^2/C), and anodic oxide forming rate (nm/s) as compared to acid electrolytes.

All details of the electrochemical parameters employed in the second part of the present study, and the corresponding results are presented in Table 2. All details of the electrochemical parameters employed in the second part of the present study, and the corresponding results are presented in Table 2.

3.3. The effect of the electrolyte concentration on the electrochemical oxide growth behaviour

The electrolyte concentration was shifted from 0.1 to 1.0 M in all test electrolytes.

An increase of the electrolyte concentration decreased the anodic forming voltage (Ar vs Ac in Fig. 10, Pc vs Pr in Fig. 11 and Ca.r vs Ca.c in Figs. 12 and 13) in all tested electrolytes. This increase also decreased the current efficiency (nm.cm^2/C) and anodic oxide forming rate (nm/s) in all tested electrolytes whereas the current efficiency (nm.cm^2/C) and anodic oxide forming rate (nm/s) slightly increased in calcium hydroxide alone (Ar vs Ac, Pc vs Pr and Ca.r vs Ca.c in Fig. 14). Furthermore, an increase of the electrolyte concentration resulted in an increase of oxide growth constant (nm/V) in acetic acid and calcium hydroxide but in a decrease of oxide growth constant (nm/V) in phosphoric acid (Fig. 14). From a quantitative viewpoint, phosphoric acid

Table 2
Summary of the electrochemical parameters and the oxide growth behaviours[a]

Sample	Concentration (M)	Voltage (V)	Current density (mA/cm^2)	Time (s)	Temperature (°C)	Charge (C/cm^2)	Current efficiency ($nm.cm^2/C$)	Oxide thickness (nm)	Growth constant (nm/V)	Anodic oxide forming rate (nm/s)
Acetic acid										
A1	0.1	40	20	8	17	0.16	386	61.77	1.54	7.72
A2	0.1	60	20	17.5	17	0.35	284	99.4	1.65	5.68
Ar	0.1	80	20	34	17	0.68	226	154.28	1.92	4.53
Acd	0.1	80	30	17	17	0.51	297	151.65	1.89	8.92
Ac	1	80	20	44	17	0.9	197	177.5	2.21	3.94
At	0.1	80	20	67	42	1.34	123	165.43	2.06	2.46
A200	0.1	80	20	27	17	0.54	281	151.65	1.89	5.61
AII	0.1	80	20	43	17	0.86	178	153.78	1.92	3.57
Phosphoric acid										
P1	1	40	10	18.5	17	0.18	374	67.45	1.68	3.64
P2	1	60	10	22	17	0.22	437	96.31	1.6	4.37
Pr	1	80	10	47	17	0.47	296	139.44	1.74	2.96
Pcd	1	80	20	10	17	0.2	717	143.56	1.79	14.35
Pc*	0.1	80	10	30	17	0.3	473	142	1.77	4.73
Pa	1	80	10	45	17	0.45	315	142	1.77	3.15
Calcium hydroxide										
Ca1	0.1	40	20	13	17	260	174	45.36	1.13	3.48
Ca2	0.1	60	20	32	17	640	99	63.9	1.06	1.99
Ca.r	0.1	80	20	47.5	17	950	96	92.01	1.15	1.93
Ca.cd	0.1	80	40	17.5	17	700	103	72.77	0.9	4.15
Ca.c	1	80	20	53.5	17	1070	101	108.77	1.35	2.03
Sodium hydroxide										
Na1	0.1	40	20	22	17	0.44	110	48.49	1.21	2.2
Na.r	0.1	60	20	65	17	1.3	53	69.2	1.15	1.06
Na3#	0.1	80	20	110	17	2.2	49	108.34	1.35	0.98
Na.cd	0.1	80	40	15.5	17	0.62	146	90.31	1.12	5.83
Na.t	0.1	60	20	88	42	1.76	43	76.32	1.27	0.87
Na.a	0.1	60	20	84	17	1.68	46	77.8	1.3	0.93
Na.200	0.1	60	20	13	17	0.26	286	74.26	1.24	5.71

[a] The abbreviations represented the used electrochemical parameters as before in each figure. Unless otherwise stated, the used electrochemical parameters are the same as the reference oxide (Ar, Pr, Ca.r and Na.r in each electrolyte). *Pc was compared to Pr. #Na3 was compared to Na.cd.

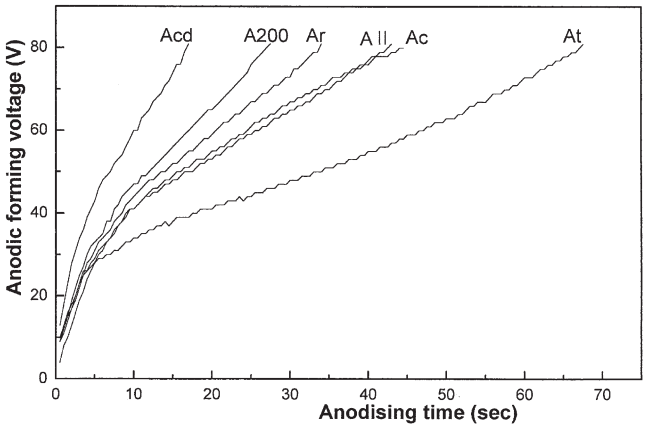

Fig. 10. The voltage to time transient curves on the Ti electrode accompanied by change of the electrochemical parameters in acetic acid. Ar is a reference oxide film formed on Ti electrode (ASTM grade 1) in 0.1 M acetic acid at 10 mA/cm^2, 17°C, 250 rpm up to 80 V for 34 s. Platinum cathodes of 80 cm^2 surface area were bilaterally used. Ac is a change of the electrolyte concentration from 0.1 to 1.0 M. Acd is a change of the current density from 20 to 30 mA/cm^2. At is a change of the electrolyte temperature from 17 to 42°C. As is 200% increase of the surface area ratio of anode to cathode by using single cathode instead of double cathode. AII is a ASTM grade 2 titanium electrode.

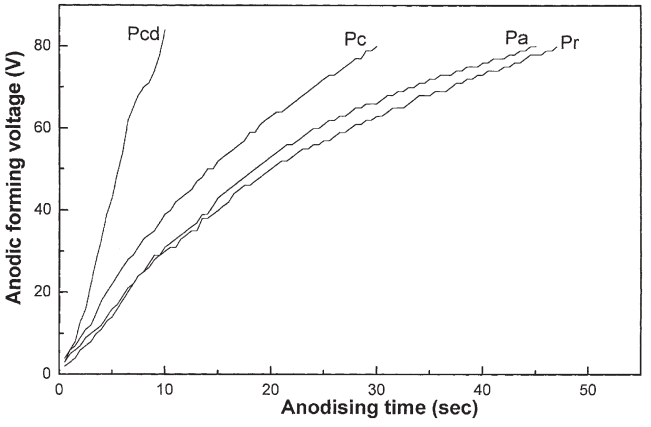

Fig. 11. The voltage to time transient curves on the Ti electrode accompanied by change of the electrochemical parameters in phosphoric acid. Pr is a reference oxide film formed Ti electrode (grade 1) in 1.0 M phosphoric acid at 10 mA/cm^2, 17°C, 250 rpm up to 80 V for 47 s. Platinum cathodes of 80 cm^2 surface area were bilaterally used. Pc is a change of the electrolyte concentration 1.0 to 0.1 M. Pcd is a change of the current density from 10 to 20 mA/cm^2. Pa is a change of the agitation speed from 250 to 800 rpm.

showed the biggest differences of current efficiency (473 vs 296 nm.cm^2/C) and anodic oxide forming rate (nm/s), but the smallest changes in oxide growth constant (1.74 vs 1.77 nm/V) by altering the electrolyte concentration from 0.1 to 1.0 M (Table 2).

3.4. The effect of the applied current density on the electrochemical oxide growth behaviours

By increasing the current density (mA/ cm^2) the anodic forming voltage (Ar vs Acd in Fig. 10, Pr vs Pcd

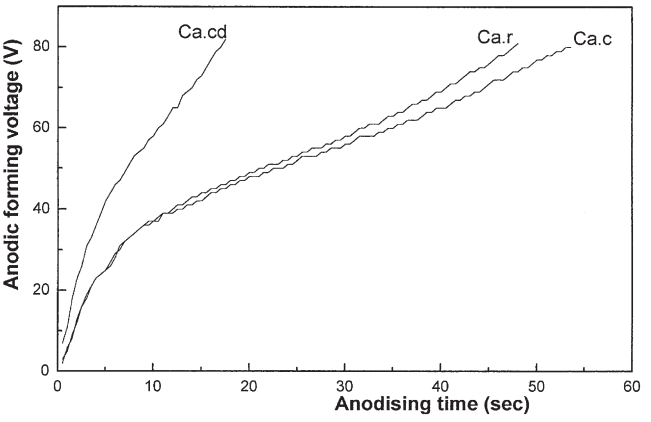

Fig. 12. The voltage to time transient curves on the Ti electrode accompanied by changes of the electrochemical parameters in calcium hydroxide. Ca.r is a reference oxide film formed on Ti electrode (grade I) in 0.1 M calcium hydroxide at 20 mA/cm^2, 17°C, 250 rpm up to 80 V for 47.5 s. Platinum cathodes of 80 cm^2 surface area were bilaterally used. Ca.c is a change of the electrolyte concentration 0.1 to 1.0 M. Ca.cd is a change of current density from 20 to 40 mA/cm^2.

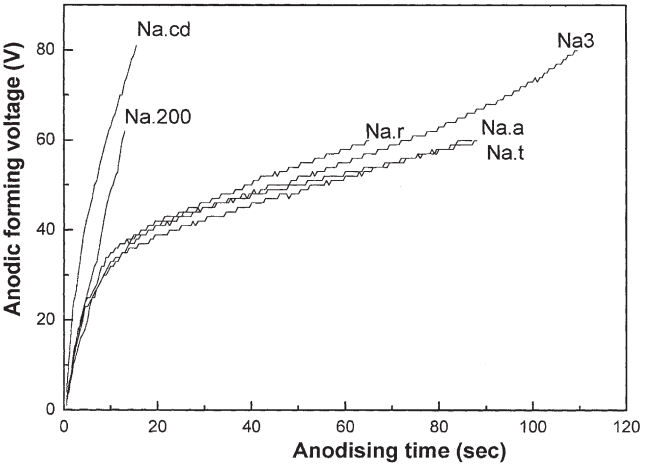

Fig. 13. The voltage to time transient curves on the Ti electrode accompanied by change of the electrochemical parameters in sodium hydroxide. Na.r is the reference oxide film formed on Ti electrode (grade I) in 0.1 M sodium hydroxide at 20 mA/cm^2, 17°C, 250 rpm up to 60 V for 110 s. Platinum cathodes of 80 cm^2 surface area were bilaterally used. Na3 is extended up to 80 V in the same anodizing conditions to Na.r and compared to Na.cd. Na.cd is a change of current density from 20 to 40 mA/cm^2 up to 80 V. Na.t is a change of the electrolyte temperature from 17 to 42°C up to 60 V. Na.a is a change of the agitation speed from 250 to 800 rpm up to 60 V. Na.200 is 200% increase of the surface area ratio of anode to cathode by double-masking 50% of the surface area of each cathode.

in Fig. 11, Ca.r vs Ca.cd in Fig. 12 and Na.3 vs Na.cd in Fig. 13), current efficiency (nm.cm^2/C) and anodic oxide forming rate (nm/s) increased for all tested electrolytes (Ar vs Acd, Pr vs Pcd, Ca.r vs Ca.cd and Na.3 vs Na.cd in Fig. 15), whereas the oxide growth constant (nm/V) decreased for all tested electrolytes except for minute increase (1.74 vs 1.79 nm/V) in phosphoric acid which slightly increased. The current efficiency

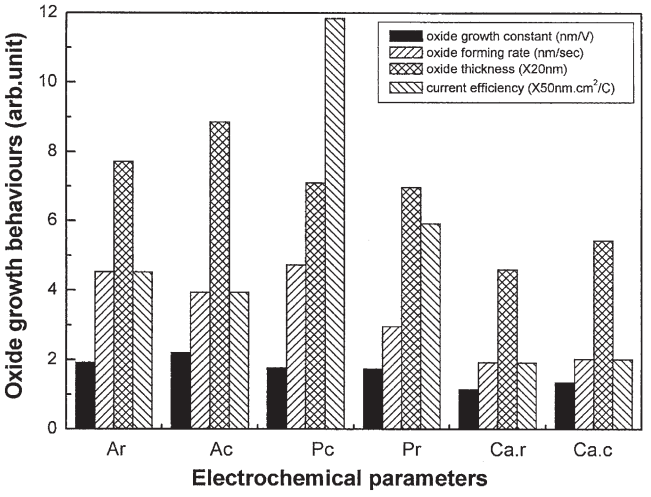

Fig. 14. The effect of the electrolyte concentration on the electrochemical oxide growth behaviours in acetic acid, phosphoric acid, calcium hydroxide, and sodium hydroxide. The nomenclatures represent the used electrochemical parameters as before.

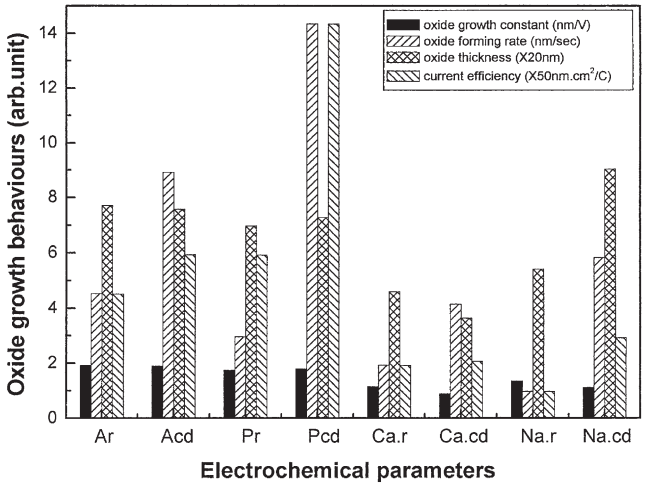

Fig. 15. The effect of the current density on the electrochemical oxide growth behaviour in acetic acid, phosphoric acid, calcium hydroxide, and sodium hydroxide. The nomenclatures represent the used electrochemical parameters as before.

(nm.cm^2/C) and anodic forming rate (nm/s) drastically increased to 242% (296 vs 717 nm.cm^2/C) and about 484% (2.96 vs 14.35 nm/s) in phosphoric acid and also increased to about 300% (49 vs 146 nm.cm^2/C) and about 594% (0.98 vs 5.83 nm/s) in sodium hydroxide, respectively (Table 2).

3.5. The effect of the electrolyte temperature on the electrochemical oxide growth behaviour

The electrolyte temperature was shifted from 17 to 42°C in acetic acid and sodium hydroxide. An increase of the electrolyte temperature resulted that the anodic forming voltage (Ar vs At in Fig. 10 and Na.r vs Na.t in Fig. 13), current efficiency (nm.cm^2/C) and anodic oxide forming rate (nm/s) decreased for both electrolytes (Ar vs At and Na.r vs Na.t in Fig. 16), whereas the oxide growth constant (nm/V) increased for both electrolytes (Ar vs At and Na.r vs Na.t in Fig. 16). In acetic acid, the increase of the electrolyte temperature most strongly influenced the current efficiency.

3.6. Effects of the agitation speed on the electrochemical oxide growth behaviours

The electrolyte temperature was shifted from 250 to 800 rpm in phosphoric acid and sodium hydroxide. An increase of the agitation speed of a stirrer did not show obvious differences (1.74 vs 1.77 nm/V) of the electrochemical oxide growth behaviours in phosphoric acid (Table 2). Sodium hydroxide showed a relative decrease of the anodic forming voltage (Na.r vs Na.a in Fig. 13), current efficiency (nm.cm^2/C) and anodic oxide forming rate (nm/s), whereas the oxide growth constant (nm/V) increased relatively (1.15 vs 1.3 nm/V) to phosphoric acid (Table 2).

3.7. The effect of the relationship (surface area ratio and location of the electrodes) between the electrodes on the electrochemical behaviours and growth behaviours

The surface area ratio of anode to cathode was increased to 200% in two ways; (1) using a single cathode instead of bilateral double cathodes shown in Fig. 1 in acetic acid (unilateral single cathode) and (2) double-masking each half of bilateral double cathodes in sodium hydroxide. The 200% increase of surface area ratio of anode to cathode resulted in increase of anodic forming voltage (Ar vs A200 in Fig. 10 and Na.r vs Na200 in

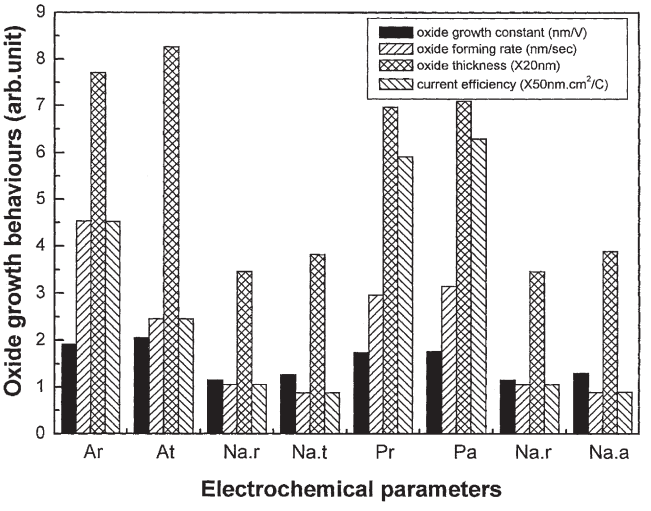

Fig. 16. The effect of the electrolyte temperature and the agitation speed on the electrochemical oxide growth behaviours in acetic acid, phosphoric acid, and sodium hydroxide. The nomenclatures represent the used electrochemical parameters as before.

Fig. 13), oxide growth constant (nm/V), current efficiency (nm.cm^2/C) and anodic oxide forming rate (nm/s) (Ar vs A200 and Na.r vs Na200 in Fig. 17) except for minor decrease (1.92 vs 1.89 nm/V) of growth constant in acetic acid.

In particular, double-masking each half of bilateral double cathodes in sodium hydroxide rose straight up anodic forming voltage with nearly a constant slope (dV/dt) (Na.r vs Na200 curve in Fig. 13). The current efficiency and anodic forming rate increased to about 540%, respectively (53 vs 286 nm.cm^2/C and 1.06 vs 5.71 nm/s) (Table 2).

3.8. The effect of the chemical composition of the titanium electrode on the electrochemical oxide growth behaviours; commercially pure (c.p.) titanium ASTM grade 1 vs grade 2

ASTM grade 2 showed a slight decrease of the anodic forming voltage (Ar vs AII in Fig. 10), current efficiency (nm.cm^2/C) and anodic oxide forming rate (nm/s) in acetic acid (Ar vs AII in Fig. 17). However, there were no obvious differences in the growth constant film(1.92 vs 1.92 nm/V) (Table 2).

4. Discussion

4.1. The colours of the galvanostatic anodic oxide films

The colouring of titanium oxide has been illustrated by the multiple beam interference theory [50]. If a light source, e.g. D 65 used in the present study, strikes the titanium oxide, there will be an interference phenomenon between the reflected beam from the oxide surface and the beam which penetrates the surface oxide and then is reflected from the interface of the surface oxide and titanium substrate. Therefore, interference colours can be influenced by non-uniformity of the oxide film in the investigated specimen. The galvanostatic oxide films prepared in the present study basically express these interference colours. The present study showed that the colours of the galvanostatic titanium oxide was principally dependent on the anodic oxide thickness. This is in agreement with previous studies [50–52]. However, our results suggest that although the galvanostatic oxide thickness is almost the same, the resultant colours can be different from the used electrolyte as well as the current density and the electrolyte concentration employed, as seen in Table 1. This is probably due to the different growth constant (nm/V) and the different anodic forming rate (nm/s) which, as previously determined numerically, are dependent on the nature of the used electrolyte as well as being altered by changes of the current density and the electrolyte concentration. In turn, these changes of growth constant (nm/V) and the anodic forming rate (nm/s) cause a change in the stoichiometry of the anodic oxide. Consequently, this non-stoichiometric layer may be responsible for the different colouring of the titanium oxide having the same thickness. Indeed, an ellipsometry study has shown the formation of an intermediate suboxide TiO_{2-x} layer between a TiO layer contacting with the titanium substrate and the TiO_2 being in the outer layer of the anodic titanium oxide [45]. Furthermore, in a Rutherford back scattering study (RBS) showed oxygen overstoichiometry in the outer layer of the anodic oxide films [53]. Another explanation for the different colouring of the titanium oxide of the same thickness may be ascribed to the different crystal structures of anodic oxide, i.e. the anatase form and the rutile form, implying changes of the density of the anodic oxide films. Even if the anodic oxide films in the anodic forming voltage up to 100 V employed in this study will consist mostly in an amorphous form, they can possibly be mixed with anatase type of the crystal structure as indicated by finding using transmission electron spectroscopy (TEM) [19,20], Raman spectroscopy [21], and X-ray absorption spectroscopy (XAS) [22]. Moreover, the different anodic oxide forming rate (nm/s) given in this study probably produces the different defect concentration profiles of the anodic oxide, i.e. the defect density [42]. In spite of the colour differences in the details, as seen in Table 1, the colours of titanium oxide can be utilized for a quick identification purposes of the resultant oxide thickness in association with the anodic forming voltage.

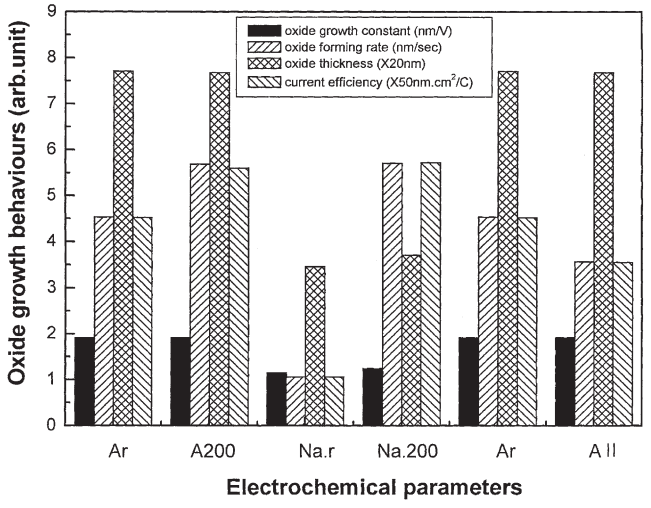

Fig. 17. The effect of the surface area ratio of anode to cathode and the different chemical composition of the titanium anode on the electrochemical oxide growth behaviours in acetic acid and sodium hydroxide. The nomenclatures represent the used electrochemical parameters as before.

4.2. The nature of the electrolytes

The relationship between the nature of an electrolyte and the electrochemical growth behaviour of the anodic

titanium oxide seems to be not fully understood. The effectiveness of an electrolyte for anodic oxidation of titanium metal appears to be largely a function of the electrolyte's activity to dissolve the anodic product [54]. Depending on the anodic conditions, different types of anodic behaviour have been observed, such as micropitting, passivity (self-passivation), uniform corrosion, and film formation by varying the concentration and temperature even in the same electrolyte [55]. It is generally assumed that the anodic oxide growth behaviour is determined by electrochemical dynamics between the ability of oxide film formation and the oxide dissolution rate given by the nature of the electrolyte. For instance, as shown in Fig. 5 (Ca and Na curve), the nature of alkaline electrolytes such as calcium hydroxide and sodium hydroxide reveals a relatively lower ability of anodic oxide formation. Therefore, anodic forming voltage corresponding to the steady state, i.e. dynamic equilibrium between the oxide formation rate and field assisted and/or chemical dissolution rate, is much lower. On the other hand, acid electrolytes such as sulphuric acid, acetic acid, and phosphoric acid, reveal that the anodic oxide formation rate overwhelmingly exceeds the dissolution rate. As a whole, electrochemical growth of the anodic titanium oxide occurs in the following hierarchy: 1 M phosphoric acid at 5 mA/cm^2 >0.1 M sulphuric acid at 15 mA/cm^2 >0.1 M acetic acid at 5 mA/cm^2 >0.1 M calcium hydroxide at 5 mA/cm^2 >0.1 M sodium hydroxide at 5 mA/cm^2. Hereby, we suggest that these results can be primarily attributed to the intrinsic nature of the electrolyte itself. At the same time, the nature of the electrolyte is exerted in a very closed connection with the electrochemical parameters such as the current density, the electrolyte concentration, conductivity, the temperature, the agitation speed, surface areas ratio of cathode to anode, etc of which results in detail are given in the next part of this discussion. It was found difficult in this study to establish a correlation between the nature of the electrolytes employed and their solubility, pH, and conductivity. So far as it is concerned with the electrolytes of which the rate of oxide film formation exceeds the dissolution rate, voltage-to-time transients (dV/dt) at a given constant current density behave typical characteristics of the galvanostatic anodizing. On commencement of anodizing, the anodic forming voltage increases almost linearly with the anodizing time up to about 80–90 V in 0.1 M sulphuric acid at 15 mA/cm^2, about 90–100 V in 0.1 M acetic acid at 5 mA/cm^2, about 40–50 V in 0.1 M calcium hydroxide at 5 mA/cm^2 and 0.1 M sodium hydroxide at 5 mA/cm^2, thereafter dielectric breakdown occurs with voltage transient with slope (dV/dt) progressively decreasing. The breakdown voltage in 1 M phosphoric acid at 5 mA/cm^2 appears to be beyond the voltage range given in this study, i.e. 100 V. These figures indicate that dielectric breakdown voltage can differ from one electrolyte to another, and also can be higher by the decrease of the electrolyte concentration. The linear increase of the forming voltage and the galvanostatic oxide thickness have been explained by the well-known high field-assisted ionic transport mechanism [56,57]. The relationship between the anodic current and the electric field strength across the anodic oxide film is described by the following equation,

$$i = A\exp(BE) \quad (1)$$

where i is the ionic current, A and B electrolytic constants, E is electric field strength and can be replaced by V/d, where V is the forming voltage and d refers to the anodic oxide thickness. During galvanostatic anodizing, in order to maintain the given constant current density, a constant field strength across the previously formed barrier film is required. As a consequence, when the oxide thickness increases with time at constant current density, the voltage across the oxide film must increase in order to maintain the field and the current density. Our experimental data presents evidently the linear increase of galvanostatic oxide thickness with the anodic forming voltage as shown in Fig. 6. This is well consistent with the above equation. Hence, so far as anodic oxide thickness of barrier film is concerned, the following equation can be induced

$$d = \alpha V \quad (2)$$

where α is growth constant (nm/V). Indeed, the growth constant has been very often used to express the oxide thickness in numerous studies. In the literature survey, the reported growth constants are controversial, and have a considerably varied range of values from 1.9 to 6.0 nm/V [19,21,22,29,53,54,58–61]. The growth constant values detected in this study are lower than in the literature data. Of course, a number of experimental variables might be carefully considered: the electrochemical parameters, the techniques used in measurement of the oxide thickness, the history of the sample preparation, the physical properties of the anodic oxide film, e.g. the density, the crystal structure, and the morphological properties, e.g. the surface homogeneity and porosity of the oxide film, etc. However, as shown in Fig. 2, measurement of the anodic oxide thickness by AES depth profiling appears to be very reliable [4,49] with a standard deviation being less than 4.0 nm of standard deviation for 109 nm in the samples of the present study, which implies uniformity of the titanium substrate (the oxide films were even barrier films without pores/craters which mainly formed before breakdown voltage). The anodic oxide thickness increases linearly with increase of the total charge passed to the oxide films, while the current efficiency (nm.cm^2/C) decreases with increase of oxide thickness. In general, the current efficiency is much higher in all the early stages of galvanostatic oxide growth before oxygen evolution. For phosphoric acid the current efficiency is almost stable (1424±75 nm.cm^2/C)

at any given charge, and shows the highest value among the electrolytes employed in this study except for the early anodizing stage in 0.1 M acetic acid at 5 mA/cm^2. For other electrolytes, however, the current efficiency decreases slightly but continuously with increase of the anodic charge (and also the anodic forming voltage). The current efficiency is generally lower in the alkaline electrolytes. Probably, one reason is attributed to the gas evolution that was empirically observed much more in alkaline electrolytes during anodizing on the surface of the titanium anode in comparison to acid electrolytes. This decreasing trend of the current efficiency has also been reported in literature [29,62]. It was likely due to the increase of oxygen evolution during galvanostatic anodizing [31], to the crystallization accompanied by increase in anodic oxide thickness [19–22], and to the increase of the field-assisted chemical dissolution by the elongation of the anodizing time [28,63].

4.3. Effects of electrochemical parameters on growth behaviour of the titanium oxide

The voltage-to-time characteristics during anodizing were highly reproducible (Figs. 10–13) except that the anodizing time up to 80 V in phosphoric acid was slightly scattered (47±4 s) (Fig. 11). From the present study, it is clear that the general changes of the electrochemical parameters have not only quantitative but also qualitative effects on the electrochemical oxide growth behaviour in terms of the galvanostatic anodic oxide thickness, anodic oxide growth constant, the current efficiency, and anodic forming rate. Of course, these behaviours are greatly dependent on the nature of the employed electrolytes, results that are in good accordance with the first part of this study.

The effect of the electrolyte concentration shows that, in general, the anodic forming voltage apparently decreases with increase of the concentration of all the electrolytes employed in this study. Therefore, the total amount of anodic charge as well as the anodizing time consumed to any preset voltages increases. This phenomenon can be explained on the basis of the 'electrical double layer' mode [23,33]. The structure of the electrical double layer is schematically shown in Fig. 18. Theoretically, it has been proposed that during electrochemical anodizing, the 'electrical double layer' forms at the oxide film/electrolyte interface, which consists of an excess or deficit of electrons on the metal side and of an excess or deficit of ions on the electrolyte side. These couplings of electrons and ions during anodizing normally result in a certain gradient of the concentration distribution of the electrolyte at the oxide film/electrolyte interface, i.e., the inner layer of the lower concentration (C–D layer in Fig. 18) and the outer layer of the higher concentration (D–E layer in Fig. 18). In this situation, if an increase of the electrolyte concentration is sufficient

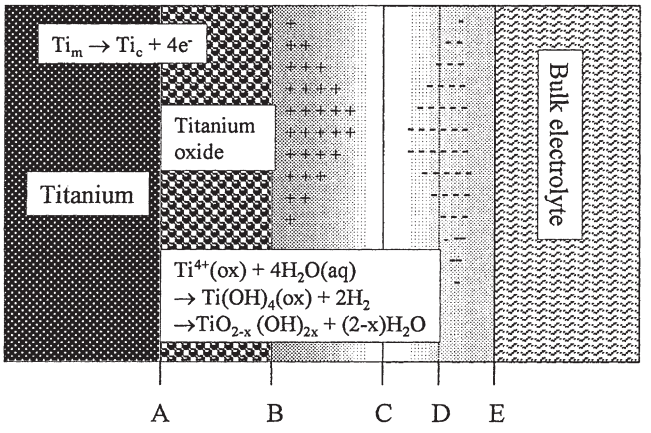

A: Metal/oxide interface
B-C: Defect layer of electrons
C: Oxide/electrolyte interface
D: Gradient line of the concentration distribution
D-E: Excess layer of anions

Fig. 18. Schematic structure of the electrical double layer at the titanium oxide/electrolyte interface. Subscripts indicate: m—metal and c—cation.

to heighten the lowered concentration of the inner layer, the electrochemical reaction at the interface accelerates and then the electrical resistance will be reduced. Eventually the anodic forming voltage decreases with increase of the electrolyte concentration. As shown in Fig. 14, by increasing the electrolyte concentration from 0.1 to 1.0 M, the oxide thickness and the growth constant increased in acetic acid and calcium hydroxide, while these parameters rather decreased in phosphoric acid. The current efficiency (nm.cm^2/C) is a possible explanation for this finding. According to Faraday's law, the current efficiency can be given by [44]:

$$\text{C.E} = \rho z F / M i . d / t \quad (3)$$

where ρ is its density, z is number of Faraday constant (F) required to form the molecular weight of the oxide M, i the current density, d thickness of the anodic oxide films, and t the anodizing time (C.E was presented as nm.cm^2/C in this study). In fact, for phosphoric acid the current efficiency (nm.cm^2/C) decreased rapidly in comparison to acetic acid and calcium hydroxide (Fig. 14). According to Eq. (1), consequently, the thickness of the resultant oxide films as well as growth constant (nm/V) decreases. Further explanation may be attributed to the differences of the anodic forming rate given in Table 2. It has been reported that rapidly grown oxide films demostrated the presence of higher defect density and revealed a higher dissolution rate [45].

The effect of the current density on the electrochemical oxide growth behaviours is not only qualitatively in opposition to the effect of the electrolyte concentration but also quantitatively much greater; an increase of the current density increases the anodic forming voltage,

while an increase of the electrolyte concentration decreases it. The relationship between the anodic current and the electric field strength across the anodic oxide film was described in Eq. (1). During galvanostatic anodic oxidation the newly formed oxide thickness dd requires an extra potential dV to maintain the field strength across the oxide films. Hence, the relation between the ratio of rise of the potential and the current density is derived from the above Faraday law (3) as follows. The rate of increase of the anodic oxide thickness is given by;

$$\mathrm{d}d/\mathrm{d}t = iM/\rho zF. \quad (4)$$

If the differential field strength E_d (dV/dd) is constant, the ratio of the potential is

$$\mathrm{d}V/\mathrm{d}t = E_d \mathrm{d}d/\mathrm{d}t = iM/\rho zF \quad (5)$$

For practical purposes, to obtain a rough idea of the order of the magnitude of dV/dt, it has been suggested that E_d varies quite slowly with i so that dV/dt is roughly proportional to i [23]. The present study shows general results well in accordance with Eqs. (4) and (5); the anodic forming voltage transient with slope (dV/dt) rises with the applied current density, the anodic oxide forming rate (d/t, nm/s) also increases with the applied current density. However, a quantitative analysis of the anodic forming voltage transient with slope (dV/dt) and the oxide forming rate (d/t, nm/s) gives considerable differences between the employed electrolytes. Regarding the anodic forming rate (nm/s), the present study shows especially high increases such as about 480% in phosphoric acid and about 600% in sodium hydroxide (Table 2). The reason for this is likely due to the differences of oxide growth constant between the electrolytes, which in turn will influence the field strength E_d(dV/dd) and the oxide forming rate (d/t, nm/s).

The effect of the electrolyte temperature on the electrochemical oxide growth behaviours appears to be a decrease of the anodic forming voltage in acetic acid as well as sodium hydroxide by increasing the electrolyte temperature. The electrochemical oxide growth is a redox reaction at the oxide film/electrolyte interface:

$$\mathrm{Ti^{4+}(ox)} + 4\mathrm{H_2O(aq)} \rightarrow \mathrm{Ti(OH)_4(ox)} + 2\mathrm{H_2} \rightarrow \mathrm{TiO_{2-x}(OH)_{2x}} + (2-x)\mathrm{H_2O}.$$

This reaction is exothermic. For instance, it has been reported that the temperature rise during anodizing is directly proportional to the electric power in the pre-breakdown stage [47], and the temperature rise for the size and shape of the specimen considered was about 1°C at 1 mA/cm^2 and 50 V, about 10°C at 10 mA/cm^2 and 50 V, and so on [23]. In other words, the above electrochemical reaction indicates a change of enthalpy $\Delta H > 0$ in the system. Therefore, thermodynamically, when the electrolyte temperature is risen, the increased temperature favours the reactants. Thereby, an increase of the electrolyte temperature will inhibit the oxide film formation and subsequently reduce the anodic forming rate (nm/s), so that the corresponding field strength E_d (dV/dd) decreases and, subsequently, the anodic forming voltage decreases. In addition, in terms of electrolyte activity, the temperature rise accelerates the ionic mobility of the used electrolytes and then decreases the electrical resistance of the electrolytes. Consequently, the anodic forming voltage will decrease and then the anodizing time reached to the preset voltage is prolonged. Indeed, the electrochemical growth behaviours presented by increasing the electrolyte temperature from 17 to 42°C are as expected above thermodynamics, and in general agreement with other studies [48,64–67]; the decrease of the anodizing time, the increase of the oxide thickness (growth constant), and the decrease of the current efficiency.

The effect of the agitation speed in 0.1 M sodium hydroxide at 20 mA/cm^2 is likely due to the gas evolution (H_2 and O_2) encountered during the dielectric breakdown. It has been reported that the dielectric breakdown is usually accompanied by gas evolution and the current efficiency is less than 100% due to gas evolution [29,31]. For phosphoric acid, the breakdown voltage in phosphoric acid is greater than the 80 V preset in this study, so gas evolution (H_2 and O_2) may be negligible. However, for calcium hydroxide, beyond approximately 45 V considered as the breakdown voltage given in this study, gas evolution (H_2 and O_2) was obviously observed. In addition, the differences of the current efficiency between 250 and 800 rpm in 1.0 M phosphoric acid was limited within about 6%, compared to approximately 18% in sodium hydroxide. This different behaviour of the gas evolution and the current efficiency related to the dielectric breakdown phenomenon may be attributed to the differences of the agitation effect between phosphoric acid and sodium hydroxide. This explanation assumes that gas evolution on the anode surface like H_2 and O_2 impedes the ionic current at the oxide/electrolyte interface and eventually increases the anodic forming voltage. Another possible explanation is regarding the effect of the current density: the gas bubble entrapped on the anode surface will reduce the surface area of the anode that takes part in the electrochemical reaction, which in turn will have effects in the form of an increase of current density and finally the anodic forming voltage will increase. Therefore, if the agitation speed is sufficient to remove the attached gas bubbles on the anode surface, the anodic forming voltage is to decrease as indicated by the result of sodium hydroxide shown in this study. As far as the anodic forming voltage is concerned, the electrical double layer represented in Fig. 18 may also be an explanatory model. When there is a cer-

tain gradient of the concentration distribution of the electrolyte at the oxide film/electrolyte interface, i.e. the inner layer of the lower concentration (C–D layer in Fig. 18) and the outer layer of the higher concentration (D–E layer in Fig. 18), this double layer acts as an electrical barrier. If the agitation speed can circulate the electrolyte enough to disturb the formation of the electrical double layer, i.e. elimination of the barrier D, the electrical resistance will be reduced and the ion–electron reactions at the oxide film/electrolyte interface will be accelerated. As a consequence, the anodic forming voltage decreases with increase of the agitation speed as shown in sodium hydroxide.

In spite of considerable effects of the ratio of the surface area of anode to cathode on the electrochemical behaviours and growth behaviours(Figs. 10 and 13Table 2), the importance of the surface area ratio of anode to cathode seems not to have been reported previously. Here, we present a probable explanation based on Ohm's law. Total resistance $R=R_c+R_{a/e}+R_e+R_{c/e}$, where R_c is the resistance of the circuit, $R_{a/e}$ the resistance of anode/electrolyte interface, R_e the resistance of electrolyte, and $R_{c/e}$ a resistance of cathode/electrolyte interface. R_c is assumed to be almost zero. Under the constant current density mode a decrease of the surface area of the cathode, e.g. to about 50% in the present study increases a corresponding $R_{c/e}$ value and consequently the voltage in cathode/electrolyte interface ($V_{c/e}$) decreases. Reciprocally the relative voltage drop of anode to cathode increases. Therefore, finally the anodizing time to reach the preset voltage gets shorter when the surface area of the cathode is reduced.

The effect of the chemical composition of the titanium electrode shows no significant difference comparing grade 1 to grade 2 in 0.1 M acetic acid at 80 V (According to ASTM standard [68], the difference of chemical composition between grade 1 and grade 2 titanium is predominantly 0.20% and 0.30% in iron content, 0.18% and 0.25% in oxygen content, respectively). For grade 2 titanium electrode the current density ($nm.cm^2/C$) and the oxide forming rate (nm/s) decreased to about 78% and the oxide thickness was almost the same, i.e. 154.3 vs 153.8 nm. In the literature, it has been reported that growth constant (nm/V) was more or less smaller for the titanium alloy than for commercially pure titanium [19,69].

In the light of the possible changes of the electrochemical oxide growth behaviours of the titanium metal presented in this study by various electrochemical parameters, further investigations are needed for a better understanding of the electrochemical and oxide growth behaviours in extensive applications to the field of the bone-anchored fixed oral and craniofacial reconstructions.

5. Conclusions

The galvanostatic anodic oxide films demonstrate the interference colours of the titanium oxide. These interference colours can be utilized for a quick identification purposes of oxide thickness which linearly increases with increased applied voltage below breakdown voltage. The growth behaviours of the titanium oxide strongly depend on the nature of the electrolytes. All electrolytes employed have particularly intrinsical specific growth constant (α, nm/V). The anodic forming voltage with slope (dV/dt) is in a hierarchial order: higher in the acid electrolytes, lower in the alkaline electrolytes. The oxide thickness increases with increase of the total charge passed to the oxide films, while the current efficiency ($nm.cm^2/C$) and the anodic oxide forming rate (nm/s) decreases with increase of the oxide thickness. The electrochemical oxide growth behaviour is greatly dependent upon the electrochemical parameters as well as the electrolytes employed, whatever electrolytes were tested in this study, in the following hierarchial order: the current density>the electrolyte concentration>the electrolyte temperature ≥the agitation speed>the chemical composition of the titanium electrode in terms of the anodic forming voltage transient with slope (dV/dt). With respect to the qualitative change of the galvanostatic oxide growth the present study reveals that the anodic forming voltage, the oxide forming rate (nm/s), and the current efficiency ($nm.cm^2/C$) increases with increase of the current density and the surface area ratio of the anode to cathode, while the anodic forming voltage, the oxide forming rate (nm/s), and the current efficiency ($nm.cm^2/C$) decreases with increase of electrolyte concentration and temperature.

Acknowledgements

The authors would like to thank all the staff in the Department of Surface Engineering, Korea Institute of Machinery and Materials for their support when using their facilities and equipment. We are grateful for grants received from the Medical Research Council (MRF), The Sylvan Foundation, The Hjalmar Svensson Research Foundation and The Wilhelm and Martina Lundgren Research Foundation.

References

[1] Brånemark PI, Hansson BO, Adell R, Breine U, Lindström U, Hallén O, Öman A. Osseointegrated implants in the treatment of the edentulous jaw. Experience from a 10-year period. Scand J Plast Reconstr Surg 1977;16(Suppl. 1):7–127.

[2] Albrektsson T, Brånemark PI, Hansson HA, Lindström J. Osseointegrated titanium implants. Acta Orthop Scand 1981;52:155–79.

[3] Kasemo B, Lausmaa J. Aspect of surface physics on titanium implants. Swed Dent J 1983;28(Suppl.):19–36.
[4] Lausmaa J, Kasemo B. Surface spectroscopic characterization of titanium implant materials. Appl Surf Sci 1990;45:133–46.
[5] Olefjord I, Hansson S. Surface analysis of four dental implant systems. Int J Oral Maxillofac Impl 1993;8:32–40.
[6] Rådegran G, Lausmaa J, Matsson L, Rolander U, Kasemo B. Preparation of ultra-thin oxide window on titanium for TEM analysis. J Elect Micr Tech 1991;19:99–106.
[7] Zitter H, Plenk HJ. The electrochemical behaviour of metallic implant materials as indicator of their biocompatibility. J Biomed Mater Res 1987;21:881–96.
[8] Williams DF. Corrosion of implant materials. Ann Rev Mater Sci 1976;6:237–65.
[9] Solar RJ, Pollack SR, Korostoff E. In vitro corrosion testing of titanium surgical implant alloys: an approach to understanding titanium release from implants. J Biomed Mater Res 1979;13:217–50.
[10] Tengvall P, Lundström I. Physico-chemical considerations of titanium as a biomaterial. Clin Mater 1992;9:115–34.
[11] Johansson CB. On tissue reactions to metal implants. Thesis, University of Göteborg, Sweden, 1991.
[12] Leonardis DD, Garg AK, Pecora GE, Andreana S. Osseointegration of rough acid etched implant: one-year follow-up of placement of 100 minimatic implants. Int J Maxillofac Impl 1997;12:65–73.
[13] Klokkevold PR, Nishimura RD, Adachi M, Caputo A. Osseointegration enhanced by etching of the titanium surface. A torque removal study in the rabbit. Clin Oral Impl Res 1997;8:442–7.
[14] D'Lima DD, Lemperle SM, Chen PC, Holes RE, Cowell CW. Bone response to implant surface morphology. J Arthroplasty 1998;13:923–8.
[15] Buser D, Nydegger T, Oxland T, Cochran DL, Schenk RK, Hirt HP, Snetivy D, Nole LP. Interface shear strength of titanium implants with a sandblasted and acid-etched surface: a biomechanical study in the maxilla of miniature pigs. J Biomed Mater Res 1999;45:75–83.
[16] Wennerberg A. On surface roughness and implant incorporation. Thesis, University of Göteborg, Sweden, 1996.
[17] Jeong Y. The structural chemistry of anodic alumina. Thesis, Corrosion and Protection centre, University of Manchester Institute of Science and Technology UK, 1993.
[18] Tabrizi R. Surface treatments of titanium and its alloy. Thesis, corrosion and protection centre, University of Manchester Institute of Science and Technology UK, 1989.
[19] Blondeau G, Froelicher M, Froment M, Hugot-Le-Goff A. Structure and growth of anodic oxide films on titanium and TA6V alloy. J Less-Comm Met 1977;56:215–22.
[20] Mattsson L and Rolander U. Structure and morphology of anodic oxide films on titanium. GIPR-264, Chalmers University of Technology, Göteborg, Sweden, 1985.
[21] Arsov LD, Kormann C, Plieth W. Electrochemical synthesis and In situ Raman spectroscopy of thin films of titanium dioxide. J Raman Spectrosc 1991;22:573–5.
[22] Fonseca C, Traverse A, Tadjeddine A, Belo MC. A characterization of titanium anodic oxides by X-ray absorption spectroscopy and grazing X-ray diffraction. J Electroanal Chem 1995;388:115–22.
[23] Young L. Anodic ocide films. London: Academic Press, 1961.
[24] Yahalom J, Zahavi J. Electrolytic breakdown crystallization of anodic oxide films on Al, Ta and Ti. Electrochim Acta 1970;15:1429–35.
[25] Ammar IA, Kamal I. Kinetics of anodic oxide-film growth on titanium—I. Acid media. Electrochim Acta 1971;16:1539–53.
[26] Ammar IA, Kamal I. Kinetics of anodic oxide-film growth on titanium—II. Neutral and alkaline media. Electrochim Acta 1971;16:1555–68.
[27] Kalra KC, Singh KC, Singh M. Formation and breakdown characteristics of anodic oxide films on valve metal. Indian J Chem 1997;36A:216–8.
[28] Armstrong RD, Harrison JA, Thirsk HR, Whitfield R. The anodic dissolution of titanium in sulfuric acid. J Electrochem Soc 1970;117:1003–4.
[29] Dyer CK, Leach JSL. Breakdown and efficiency of anodic oxide growth on titanium. J Electrochem Soc 1978;125:1032–8.
[30] Albella JM, Montero I, Martinez-Duart JM. A theory of avalanche breakdown during anodic oxidation. Electrochim Acta 1987;32:255–8.
[31] Delplancke JL, Winand R. Galvanostatic anodization of titanium—II. Reactions efficiencies and electrochemical behaviour model. Electrochim Acta 1988;33:1551–9.
[32] Hwang BJ, Hwang JR. Kinetic model of anodic oxidation of titanium in sulphuric acid. J Appl Electrochem 1993;23:1056–62.
[33] Sato N. A theory for breakdown of anodic oxide films on metals. Electrochim Acta 1971;16:1683–92.
[34] Yahalom J. The role of the film/electrolyte interface in anodic breakdown. In: Alwitt SR, editor. Proceedings of the Symposium on Oxide–electrolyte Interfaces, Massachusetts, 1973.
[35] El Kader MA, El Wahab FMA, El Shayeb HA, Kheder MGA. Oxide film thickening on titanium in aqueous solution in relation to anion type and concentration. Br Corros J 1981;16:111–4.
[36] Leach JSL, Pearson BR. Crystallization in anodic oxide films. Corros Sci 1988;28:43–56.
[37] Mikula M, Blecha J, Ceppan M. Photoelectrochemical properties of anodic TiO_2 layers prepared by various current density. J Electrochem Soc 1992;139:3470–4.
[38] Aladjem A. Anodic oxidation of titanium and its alloy. J Mater Sci 1973;8:688–704.
[39] Politi A, Jouve G, Lacombe P. Cinétiques de croissance et propriétés de films anodiques formés sur le titane. J Less-Comm Met 1977;56:263–8.
[40] McAleer JF, Peter LM. Photocurrent spectroscopy of anodic oxide films on titanium. Faraday Disc Roy Soc Chem 1980;70:67–80.
[41] Delplancke JL, Winand R. Galvanostatic anodization of titanium—I. Structures and compositions of the anodic films. Electrochim Acta 1988;33:1539–49.
[42] Blackwood DJ, Petter LM. The influence of growth rate on the properties of anodic oxide films on titanium. Electrochim Acta 1989;34:1505–11.
[43] Serruys Y, Sakout T, Gorse D. Anodic oxidation of titanium in 1 M H_2SO_4, studied by Rutherford backscattering. Surf Sci 1993;282:279–87.
[44] Heber KV. Studies porous Al_2O_3 growth—II. Ionic conduction. Electrochim Acta 1978;23:135–9.
[45] Blackwood DJ, Greef R, Peter LM. An ellipsometric study of the growth and open-circuit dissolution of the anodic oxide film on titanium. Electrochim Acta 1989;34:875–80.
[46] Guntherschulze A, Betz H. Die bewegung der ionengitter von isolatoren bei extremen elektrischen feldstärken. Z Phys 1934;92:367–74.
[47] Bacarella AL, Gadiyar HS, Sutton AL. Anodic film growth on titanium at temperatures from 200°C to 257°C. J Electrochem Soc 1981;128:1531–7.
[48] Jouve G, Leach JSL. The increase in temperature of the anodic film formed on titanium during growth in acid media. Thin Sol Films 1983;110:263–73.
[49] Mathieu HJ, Mathieu JB, McClure DE, Landolt D. Beam effects in Auger electron spectroscopy analysis of titanium oxide films. J Vac Sci Technol 1977;14:1023–8.
[50] Delplancke JL, Degrez M, Fontana A, Winand R. Self-colour anodizing of titanium. Surf Technol 1982;16:153–62.
[51] Cotton JB, Hayfield PCS. Decorative finishes on titanium. Trans Inst Met Finish 1967;45:48–52.

[52] Geduld H. Anodizing titanium. Met Finish 1967;65:62–6.
[53] Serruys Y, Sakout T, Gorse D. Anodic oxidation of titanium in 1 M H_2SO_4, studied by Rutherford backscattering. Surf Sci 1993;282:279–87.
[54] Sibert ME. Electrochemical oxidation of titanium surfaces. J Electrochem Soc 1963;110:65–71.
[55] Piggott AR, Leckie H, Shreir LL. Anodic polarization of Ti in formic acid—anodic behaviour of Ti in relation to anodizing condition. Corros Sci 1965;5:165–84.
[56] Vermilyea DA. The kinetics of formation and structure of anodic oxide films on tantalum. Acta Met 1953;1:282–94.
[57] Young L. Anodic oxide films on tantalum electrodes. Trans Faraday Soc 1954;50:159–71.
[58] Aladjem A. Anodic oxidation of titanium and its alloy. J Mater Sci 1973;8:688–704.
[59] Politi A, Jouve G, Lacombe P. Cinétiques de croissance et propriétés de films anodiques formés sur le titane. J Less-Comm Met 1977;56:263–8.
[60] Torresi RM, Camara OR, De Pauli CP, Giordano MC. Hydrogen evoluation reaction on anodic titanium oxide films. Electrochim Acta 1987;32:1291–301.
[61] Kozolowski M, Smyrl WH, Atanasovska L, Atanasovska R. Local film thickness and photoresponse of thin anodic TiO_2 films on polycrystalline titanium. Electrochim Acta 1989;34:1763–8.
[62] Ohtsuka T, Masuda M, Sato N. Ellipsometric study of anodic oxide films on titanium in hydrochloric acid, sulphuric acid, and phosphate solution. J Electrochem Soc 1985;132:787–92.
[63] Averill AF. Anodic dissolution of titanium in HCl–methanol solution. Thesis, University of Manchester of Science and Technology UK, 1966.
[64] Mazhar AA. Effect of temperature on the formation and dissolution of anodic oxide films on titanium in acid solutions. J Appl Electrochem 1990;20:494–9.
[65] Magnussen ND. Characterization of anodic oxide film. Thesis, Texas A&M University USA, 1991.
[66] Kalra KC, Singh KC, Singh M. Ionic conduction in anodic oxide films on titanium in mixed solutions of aqueous electrolytes and diethylene glycol. Thin Sol Films 1994;239:99–103.
[67] Shibata T, Zhu YC. The effect of temperature on the growth of anodic oxide film on titanium. Corros Sci 1995;37:134–44.
[68] Annual book of ASTM standard. ASTM, 1998.
[69] Tabrizi R. Surface treatments of titanium and its alloy. Thesis, Corrosion and Protection centre, University of Manchester Institute of Science and Technology, UK, 1989.